

Evaluation of Microstructural Characteristics of High-Si Al Alloy Cylindrical Samples Produced by Rheological Squeeze Casting with Bottom-Up Filling and Flow State Analysis of the Alloy Semi-Solid Slurries

Ying Xiao^a, Shuaiying Xi^a, Guodong Ma^a, Lu Li^{a,b*} , Yongkun Li^a, Qiuping Wang^a, Fan Xiao^c,
Rongfeng Zhou^{a,b}, Yehua Jiang^a

^aKunming University of Science and Technology, Faculty of Material Science and Engineering, Xishan, Kunming, China

^bKunming University of Science and Technology, Research Center for Analysis and Measurement, Xishan, Kunming, China

^cJiangxi Jiangling Group New Energy Vehicle Co., Ltd, Jiangxi, Nanchang, China

Received: December 03, 2019; Revised: April 30, 2020; Accepted: May 5, 2020

The microstructures of high-Si Al alloy cylindrical samples produced by rheological squeeze-casting with bottom-up filling were investigated. The effect of process parameters on the distribution of hard phases (primary Si and Fe-rich phase) was evaluated, and flow characteristics of semi-solid slurry of high-Si Al alloy were investigated. Differences in volume fractions (VFs) of hard phases between the middle and upper layers of cylindrical samples decreased as the squeezing speed increased. Moreover, the flow state of the semi-solid alloy slurry transitioned from laminar to turbulent flow as the squeezing speed was increased. Movement of gases throughout the semi-solid alloy slurry filling process was analysed under different process parameters. The results provide insights for improving rheological casting of high-Si Al alloy and other Al matrix composites.

Keywords: High-Si Al alloy, rheological squeeze casting, casting defects, microstructure, semi-solid slurry, flow characteristics.

1. Introduction

High Si Al alloys (hypereutectic Al-Si alloys) are alloy systems with Al and Si as the main elements, for example, the commonly used commercial alloy A390. Solidification microstructures of this series of alloys are mainly comprised of primary Si, primary α -Al, and eutectic phases^{1,2}. The size and shape of primary Si have a large influence on the final properties (both mechanical and wear properties) of hypereutectic Al-Si alloys^{3,4}. Therefore, it is necessary to conduct modification treatment to refine and homogenize the primary Si phases through melt controlled cooling technology for realizing the application of this alloy⁵⁻⁷. Furthermore, hypereutectic alloys have a wide temperature range in which the Si phase and liquid phase can coexist, and this can easily lead to gas and shrinkage porosity during squeeze casting or die-casting⁸. These distinct material characteristics and material forming properties greatly limit the commercial application of high Si Al alloy.

Squeeze casting is a special casting technique that combines the advantages of high-pressure die casting and forging techniques by controlling the mould filling and solidification process of metal melts under high pressure⁹. The filling pressure is directly applied to the whole liquid surface of the metal melt resulting in materials with improved mechanical properties. Key parameters of the process

include the filling rate, final forming pressure, and mould temperature¹⁰.

Since metal melt filling is conducted under high pressure, squeeze casting is suitable for semi-solid melt forming of alloys with high apparent viscosities. Moreover, the squeeze casting process can effectively avoid the defects caused by solidification during the liquid metal filling process¹¹. When the metal melt is replaced by a semi-solid slurry, the process is referred to as semi-solid rheological forming or rheoforming.

Researchers previously investigated melt slurry preparation technologies for use in refining the primary Si phase of high Si Al alloy and found that high-viscosity slurries and low forming temperatures produce cast parts with fewer defects¹², however, subsequent microstructural investigations showed that semi-solid slurries of high Si Al alloys are mainly composed of near-liquid structures with a large number of suspended primary Si particles¹³⁻¹⁶. Small primary Si phases form agglomerates within the liquid phase at different positions that can significantly affect the performance of cast parts. In addition, the distribution of primary Si is random and difficult to control.

In recent years, some scholars have focused on the sensitivity of semi-solid cast parts to microstructural segregation. Vieira and Ferrante designed a simple back-extrusion test to assess segregation of thixocast Al-Si alloy¹⁷. Niroumand analysed the effect of the solid fraction of primary particles on the

*e-mail: liluchina@kust.edu.cn

structure and liquid segregation behaviour of cup-shaped semi-solid rheo-squeeze cast parts of hypoeutectic Al-Si alloy¹⁸.

According to the previous research results, semi-solid rheological squeeze casting technology can overcome certain forming problems encountered when using high-Si Al alloys with high brittleness. In addition, causes of segregation in high-Si Al alloy semi-solid squeeze cast parts and the related technological parameters were analysed, to improve the process and produce high-quality castings with uniform performance.

In this study, the quality and microstructure of squeeze-cast parts produced by use of the bottom-up filling method, and possible causes of defects, were analysed. Microstructures of the upper, middle, and lower sections of cylindrical cast samples were examined, and the degree of liquid phase segregation was evaluated. Flow states of the semi-solid slurry were also elucidated by examining the microstructures obtained using different process parameters

2. Experimental Procedure

2.1 Preparation of semi-solid alloy slurry

High Si Al alloy was formed in a resistance furnace by melting industrial pure Al (99.9%), metallic Si (98%, the rest being combustion accelerants), Fe (75%, the rest being combustion accelerants), and Mn (75%, the rest being combustion accelerants). The final alloy composition is summarised in Table 1. High-Si Al alloy semi-solid slurry was prepared by rotating-rod induced nucleation¹⁹. The device used to prepare the semi-solid slurry comprised: a speed motor, cooling system, pouring cup, tin-bronze rotary bar, environmental temperature control system, and pulping chamber (Figure 1). It comprised a speed motor - 1, cooling system - 2, pouring cup - 3, tin-bronze rotary bar - 4,

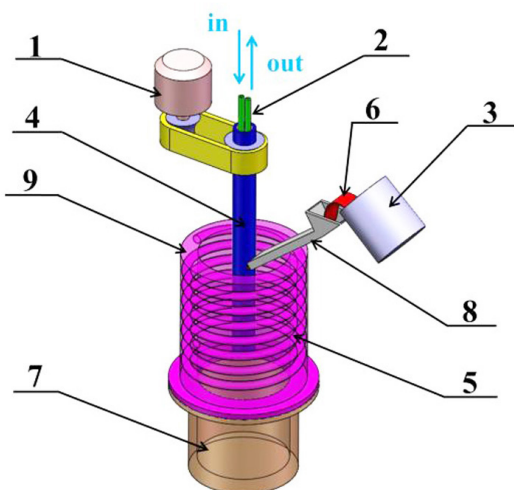


Figure 1. Schematic diagram of pulping device of rotating-rod induced nucleation method.

Table 1. Chemical compositions of the experimental alloys (wt. %).

Sample	Si/%	Fe/%	Mn/%	Al/%
Al-25Si-2Fe-1.4Mn	24.6	1.9	1.4	Balance

environmental temperature control system - 5 pulping chamber, molten melt - 6, crucible - 7, hopper - 8, and sleeve - 9. The hollow rotary bar had a diameter of 75 mm with an internal continuous drainage system for cooling and an adjustable speed of up to 2500 rpm.

2.2 Mould and process parameters for rheofforming

Semi-solid squeeze casting with bottom-up filling was adopted and the filling direction was vertically upward (Figure 2). Cylindrical samples with a height of 130 mm, outside diameter of 80 mm, and 10 mm thickness were produced by semi-solid squeeze casting. A schematic of the semi-solid forming mould is shown in Figure 2a and a photograph thereof in Figure 2b.

Rheofforming of the high Si Al alloy slurry was carried out: 1) The mould was cleaned and dried, then sprayed with a mould release agent; 2) The mould was then sealed and preheated at 250 ± 10 °C; 3) Squeeze-casting parameters were set, the mould was opened, and semi-solid slurry was poured into the barrel and the mould was closed; 4) To complete the squeeze-casting process, the pressure was maintained for 10 s, then the mould was re-opened and the cast part removed. Process parameters are listed in Table 2.

2.3 Microstructural analysis

For microstructural analysis, sections of the cylindrical samples (Figure 2c) were cut along the axial direction, and the upper, middle, and lower sections of the cylinder were etched in 0.5% HF solution and observed under a Leica optical metallographic microscope.

Criteria for evaluating the degree hard phases refinement and distribution were based on the equivalent diameter (ED) and the volume fraction (VF). Image pro-plus 2D image analysis software was used to analyze the microstructure of samples produced using different process parameters. The ED of hard phases was calculated²⁰:

$$ED = \frac{\sum_{i=1}^N \sqrt{4A_i} / \pi}{N} \quad (1)$$

where N is the total number of particles, A_i is the area of the particle i.

3. Results and Discussion

3.1 Defects of semi-solid squeeze-cast parts

Figure 3 illustrates images of high-Si Al-Si alloy squeeze-cast parts produced using different process parameters. Shrinkage porosity can be observed at the bottom section (the final solidification position) of samples produced at a squeezing speed of 8 mm/s and applied pressure of 100 MPa (Figure 3a). A large amount of gas porosity can be observed in the middle sections of samples formed at a squeezing speed of 24 mm/s and squeezing pressure of 100 MPa, as a result of increasing falling speed of the punch and a large amount of gas in the slurry (Figure 3c).

Process changes lead in large differences in porosity from Figure 3f, several tiny holes can be observed in the cast part formed at a squeeze rate of 24 mm/s and final pressure of 130 MPa. The interior of rheofformed samples is relatively

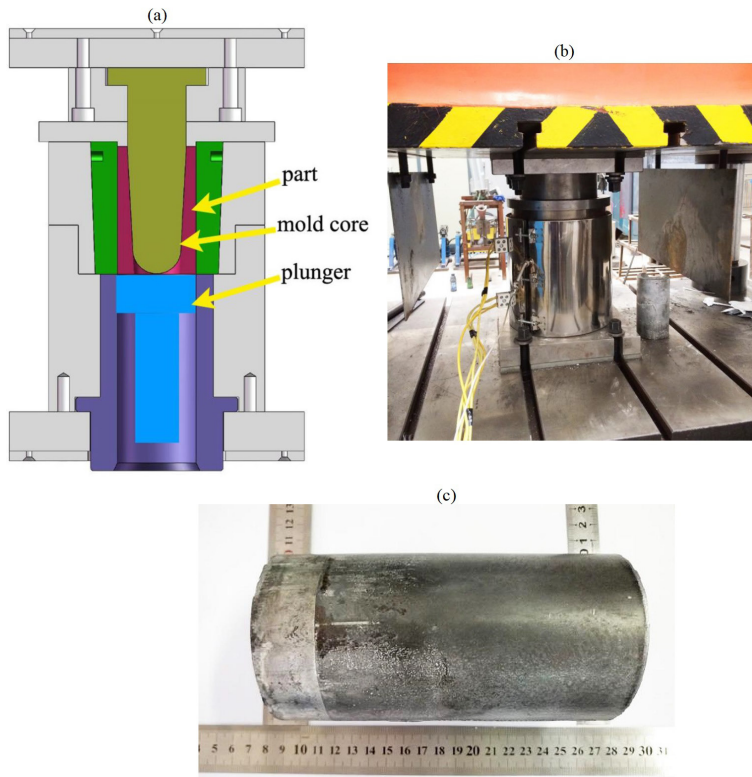


Figure 2. Semi-solid squeeze casting mold with bottom filling: (a) Schematic of mold; (b) Image of mold; (c) Image of the cylindrical simple.

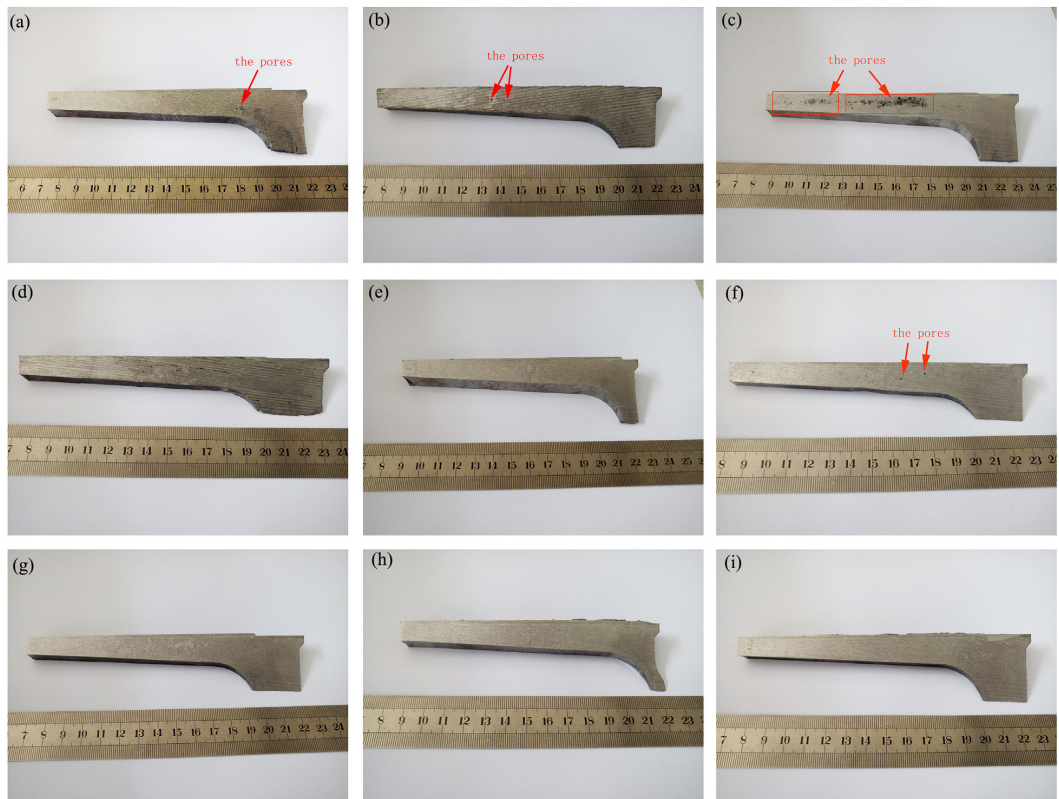


Figure 3. Section sketch of high Si Al alloy by different process parameter of rheological squeeze casting (a) 8 mm/s, 100 MPa; (b) 16 mm/s, 100 MPa; (c) 24 mm/s, 100 MPa; (d) 8 mm/s, 130 MPa; (e) 16 mm/s, 130 MPa; (f) 24 mm/s, 130 MPa; (g) 8 mm/s, 160 MPa; (h) 16 mm/s, 160 MPa; (i) 24 mm/s, 160 MPa.

compact, particularly in specimens obtained using a final pressure of 160 MPa. In conventional liquid squeeze-casting, alloy melts are fed under a sufficiently large forming pressure during the solidification process. To eliminate defects in cast parts, resistance of the solidified shell and nucleation solid phase structures of the slurry must be offset during the semi-solid filling process.

3.2 Effect of forming pressure on microstructural characteristics of hard phases

Figure 4 shows microstructures of rheoformed samples produced using three different applied pressures with squeezing speed of 16 mm/s. With a squeezing pressure of 160 MPa, hard phase particles appear a granular with the smallest equivalent

Table 2. The technological parameters of rheological squeeze casting.

No.	squeeze pressure (MPa)	squeeze speed (mm/s)
1	100	8
2	100	16
3	100	24
4	130	8
5	130	16
6	130	24
7	160	8
8	160	16
9	160	24

diameter and highest roundness. Meanwhile, the ED of hard phases is higher in upper sections of the parts compared to the middle and bottom of the longitudinal sections. It is worth noting that the number of hard phase particles per unit area increases as the forming pressure is increased.

As the applied pressure was increased, the average ED of hard phase particles in the microstructure decreased, the shape factor gradually increased, and particles become rounder and more uniform (Figure 4). During the semi-solid squeeze-casting process, the relationship between the alloy melt pressure and nucleation energy is given by²¹:

$$\Delta G = 32\sigma_{LS}T_m / (L_m\Delta T + K\xi T_m P)^2 \quad (2)$$

where ΔG is the critical nucleation energy, σ_{LS} represents the liquid-solid surface tension, T_m is the melting temperature of the alloy, L_m is the latent heat, and ΔT is the degree of undercooling.

According to Equation 2, increasing applied pressure reduces the critical nucleation energy, which is equivalent to increasing the nucleation of Si phases.

3.3 Effect of rheological squeeze rate on axial distribution of hard phases

Microstructures of rheoformed samples produced at a casting pressure of 160 MPa and squeeze rates of 8 mm/s, 16 mm/s or 24 mm/s are demonstrated in Figure 5.

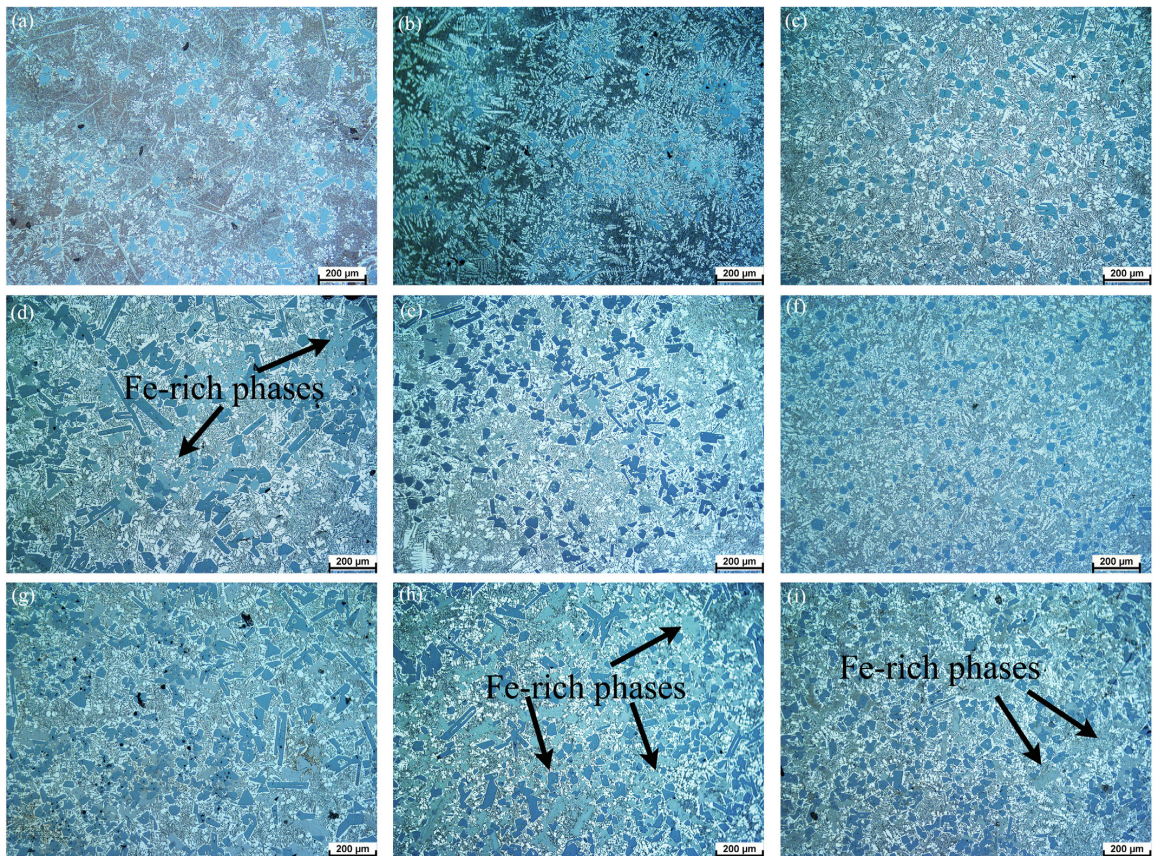


Figure 4. Microstructure of high Si Al alloy cylinder liner at different squeeze pressure (a, d, g) 16 mm/s, 100 MPa;(b, e, h) 16 mm/s, 130 MPa;(c, f, i) 16 mm/s, 160 MPa.

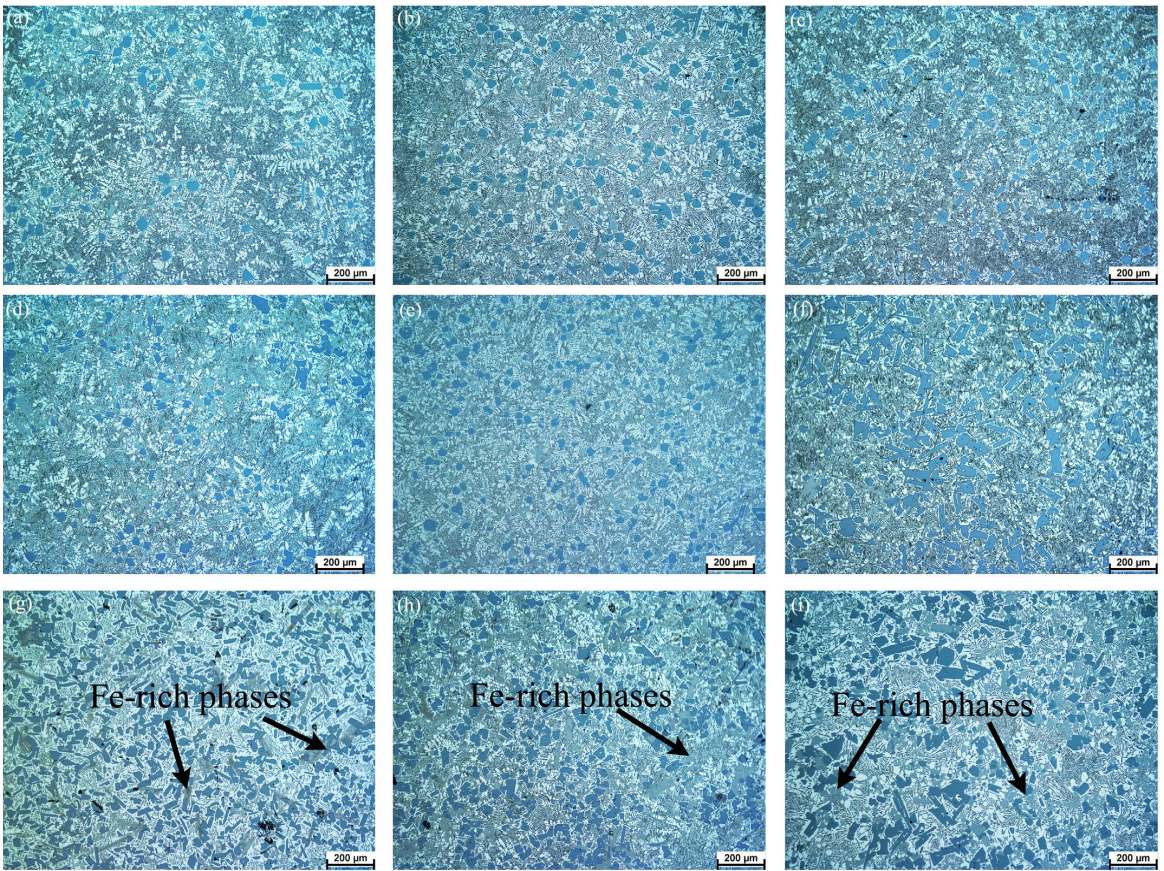


Figure 5. Microstructure of high Si Al alloy cylinder samples at different squeeze rate (a, d, g) 8 mm/s, 160 MPa (b, e, h) 16 mm/s, 160 MPa (c, f, i) 24 mm/s, 160 MPa.

VFs of hard phases in the upper, middle, and bottom sections of the samples were significantly different when the falling speed of the punch was 8 mm/s (Figure 5a, d, g). The lowest VF was found in the hard phase at the upper section of the samples (fluid level filling front) and the densest distribution of hard phases was observed in the bottom. In addition, the ED of hard phase particles in the upper section of the samples was smaller than that in the middle and bottom sections. At a squeeze rate of 16 mm/s (Figure 5b, e, h), differences in the VF of hard phase observed in the longitudinal sections at each position decreased. Based on this trend, the difference in VF was lowest at a squeeze rate of 24 mm/s (Figure 5c, f, i), and the distribution of the hard phase was more uniform in the axial direction.

Figure 6 shows the axial (filling direction) distribution of hard phase (primary Si particles and blocky Fe-rich phase) of rheological squeeze-cast high-Si Al alloy samples with different rheoforming parameters. The axial distributions of the hard phase of high-Si Al alloy samples produced using different casting pressures at an extrusion rate of 16 mm/s are depicted in Figure 6a. Similarly, the axial distributions under different squeeze rates at a casting pressure of 160 MPa are illustrated in Figure 6b. In general, the axial distribution of VF of the hard phases increases from small to large from the upper to middle to bottom of the sections.

From Figure 6a, the influence of casting pressure on the VF of hard phases is clearly observed in the same positions. The resulting semi-solid slurry has a low solid fraction (about 20%) and mainly consists of hard phases suspended in a liquid phase, however, the hard phase is discontinuous, therefore, the strength of the skeleton formed by the of solid phase is low. Under low pressures, the liquid phase is concentrated in the top of the part, causing the VF of hard phases to remain unchanged with increasing squeezing pressure.

Combined with metallographic and statistical data presented in Figure 5 and Figure 6b, it is concluded that the squeezing speed excited little influence on the VF of hard phases in the bottom of the part, but significantly influenced the VF of hard phases in the middle and upper sections of the part. At a lower squeezing speed (8 mm/s), differences between the VF of hard phases in the upper versus the middle and bottom were 3% and 18%, respectively. As the squeezing speed was increased to 16 mm/s, the differences were 5% and 11%, respectively. At 24 mm/s, the difference between the VF of hard phases in the middle and bottom sections was reduced to 6%, and increased to 10% between the upper and middle sections.

In this study, the VF of solid phases in the semi-solid alloy slurry is about 20%, which is a quasi-liquid slurry. In multiphase systems, solid phases suspended in a flowing

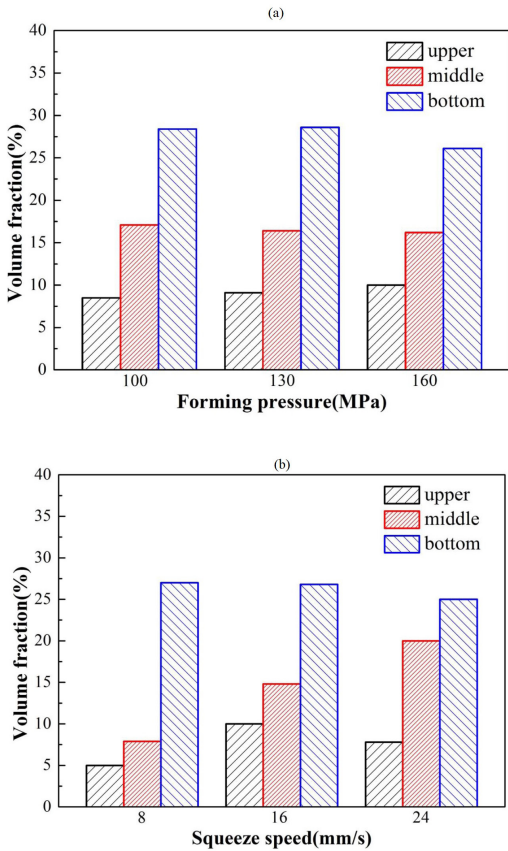


Figure 6. Distribution of hard phases in the axial of high Si Al alloy cylinder samples formed at different squeeze pressure (a) and different squeeze rate (b).

liquid phase are subjected to drag forces and solid particles flow within the liquid phase and are subjected to drag force F_D ²²:

$$F_D = C_D \frac{\rho A v^2}{2} \quad (3)$$

Based on Equation 3 (Evet et al.²²), the hard phase can be approximately regarded as spherical and the velocity component can be ignored. Coefficient C_D is related to the shape of solid phase, and was assumed to be constant in the present study; therefore, the drag force acting on the hard phase was proportional only to the liquid velocity. Therefore, as the punch speed increased, the drag force on the hard phase increased, causing particles with larger diameters to move. Moreover, as the difference between the drag force acting on the hard phase and the force due to gravity decreased, the hard phase was driven in the direction of negative pressure.

3.4 Effect of rheological filling rate on radial distribution of hard phases

Figure 7 shows the radial microstructure of samples produced at a rheological forming pressure of 160 MPa and squeezing speeds of 8 mm/s, 16 mm/s, and 24 mm/s. Pores were dispersed in the radial direction and moved towards the outer cast surface as the squeeze rate increased. Only a few random pores could be observed on the outermost surface of cast samples when the filling rate reached 24 mm/s.

It was worth noting that an agglomeration zone appeared within the liquid phase parallel to the mould-filling direction, and increased in area as the squeeze rate increased resulting in the radial distribution of hard phases.

There are two possible internal flow states: laminar flow and turbulent flow²³. Laminar flow can be thought of

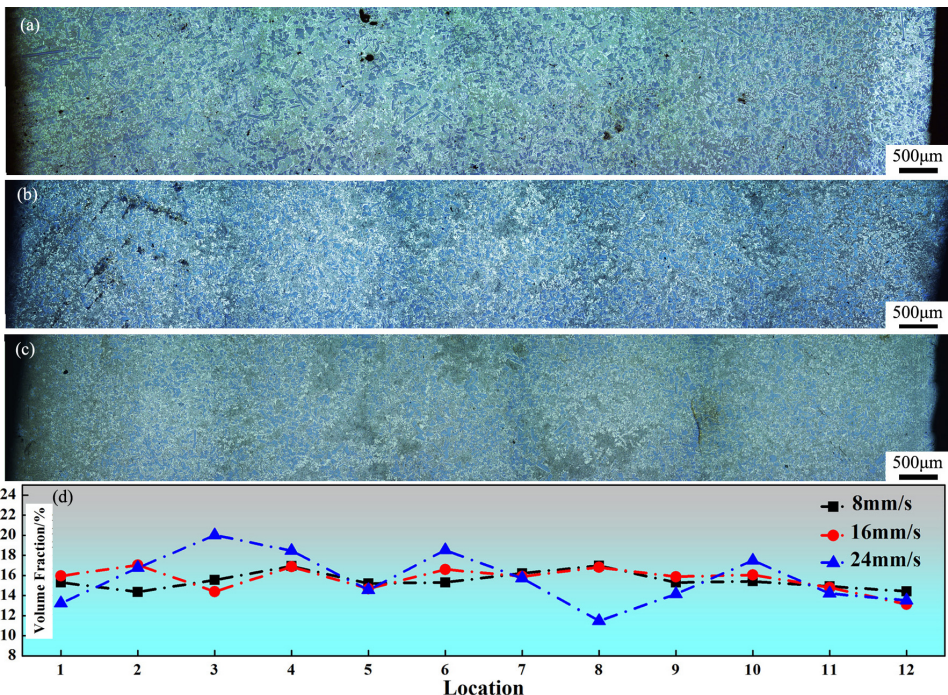


Figure 7. Hard phases distribution in radial of rheological squeeze casting high Si Al alloy cylinder samples at different process parameters (a) 8 mm/s, 160 MPa; (b) 16 mm/s, 160 MPa; (c) 24 mm/s, 160 MPa; (d) Volume fraction statistics of hard phases.

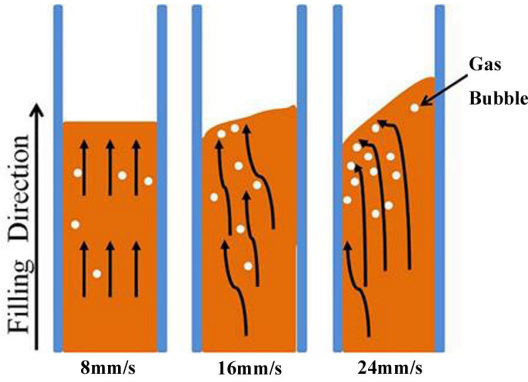


Figure 8. Schematic diagram of fluid flow state: (a) laminar flow, 8 mm/s; (b) undefined, 16 mm/s; (c) turbulent flow, 24 mm/s.

as filaments of fluid moving smoothly along the main flow direction without mixing. In contrast, turbulent flow results in the exchange of material between fluid filaments in the direction perpendicular to the main direction of flow. Reynolds number, or Re , is used to determine the internal fluid flow state, defined as the ratio of inertial to viscous forces²⁴:

$$Re = \frac{\rho D^n g^{(2-n)}}{\eta} \quad (4)$$

where ρ is the fluid density (kg m^{-3}), D is the hydraulic diameter of the runner (m), n is the fluid power law index, g represents the fluid flow rate (m s^{-1}), and η is the fluid viscosity ($\text{kg m}^{-1} \cdot \text{s}^{-1}$).

For a Newtonian fluid ($n = 1$, where n is the solid phase fraction), the internal flow state is considered laminar when Re is less than 2300, however, the criterion does not apply to non-Newtonian fluids^{25,26}. The critical Re for transition from laminar flow to turbulent flow in a non-Newtonian fluid is a function of the power law index, therefore, the critical Re for a semi-solid metal ($0 < n < 1$) is influenced by the power law index, which mainly depends on the solid fraction^{25,27}.

In present work, the solid phase fraction in the slurry is approximated as constant. At a squeeze rate of 24 mm/s (Figure 7c), a large agglomeration zone appeared in the liquid phase along the radial direction of casting with turbulence characteristics. Therefore, based on the elongational flow conditions considered in this study, the radial force inside semi-solid slurry will increase as the filling rate increases.

Hu et al.²⁸ found that internal gases gradually move toward the free liquid surface as the filling rate of semi-solid A312 alloy slurry increases. In the present study, it was therefore inferred that the free liquid level of slurry changed with as the filling rate, which caused gases in the slurry to flow to the outside of the pipe wall (Figure 8); however, the hard phase was not driven by the radial component of the drag force to outside the wall of the cast part due to the insufficient hard-phase content.

4. Conclusion

In this study, rheological squeeze casting of high-Si Al alloy slurries was performed with bottom-up filling and cylindrical samples were obtained. The influence of rheological

casting parameters on microstructures of the upper, middle, and lower sections of cast parts was analyzed. Based on the results, the following conclusions can be drawn:

1. The rheological squeeze casting process influences the microstructure of high-Si Al alloy. When the squeeze casting process parameters are defined, the ED of hard phase particles generally conforms to the rule: $ED_{\text{upper}} < ED_{\text{middle}} < ED_{\text{bottom}}$. Furthermore, hard phase particles in the upper section of samples have higher roundness. The size and shape (roundness) of hard phases are mainly affected by the casting pressure. The mould filling rate mainly influences the distribution of hard phases in the alloy slurry, in particular, differences between the VF of hard phase particles in the middle and upper sections of the cast part decrease as the mould filling rate increases.
2. Microstructural characteristics of rheological squeeze-cast samples produced at a forming pressure of 160 MPa and forming rates of 8, 16, and 24 mm/s were examined. Microstructures exhibited liquid flow zones with agglomeration zone and irregular distributions. Moreover, flow regimes of the semi-solid alloy slurry transition from laminar to turbulent flow as the squeezing speed increases.
3. The distribution of shrinkage porosities in cast samples will depend on the shape of the free liquid surface of the slurry. More specifically, higher slurry filling speeds result in increased inclination of the free liquid surface, which intensifies radial flow of slurry and promotes radial movement of gases toward the outer walls of cast cylindrical samples.

5. Acknowledgement

The authors acknowledge funding for this research from National Natural Science Foundation of China (51505205), High-tech industry development project of Yunnan Province (201802). This work is supported by the National and Local Joint Engineering Laboratory of Advanced Metal Solidification Forming and Equipment Technology, Kunming University of Science and Technology. Analytic & Testing Research Center of Yunnan, Kunming, China.

6. References

1. Kim SB, Cho YH, Jung JG, Yoon WH, Lee YK, Lee JM. Microstructure-strengthening interrelationship of an ultrasonically treated hypereutectic Al-Si (A390) alloy. *Met Mater Int*. 2018;24:1376-85.
2. Cui XI, Wu YY, Liu XF. Microstructural characterization and mechanical properties of VB₂/A390 composite alloy. *J Mater Sci Technol*. 2015;31:1027-33.
3. Li L, Geng BY, Wang QP, Zhou RF, Jiang YH. Rheo-squeeze casting of high-silicon aluminium alloy pipes with gradient structures and their mechanical properties. *Mater Res*. 2018;21:e20180165.
4. Haghayeghi R, Zoqui EJ, Timelli G. Enhanced refinement and modification via self-inoculation of Si phase in a hypereutectic aluminium alloy. *J Mater Process Technol*. 2018;252:294-303.
5. Yan PY, Mao WM, Fan J, Wang BK. Simultaneous refinement of primary si and modification of eutectic Si in A390 alloy

- assisting by Sr-Modifier and serpentine pouring channel process. *Materials* (Basel). 2019;12:3109.
6. Nie JF, Zhao YH, Li YS, Wang F, Yang HB, Hu KQ, et al. Reactive synthesis of hexagonal $Ti_5P_{3.16}$ crystals and their heterogenous nucleating mechanism on primary Si. *J Alloys Compd.* 2019;777:8-17.
 7. Li L, Zhou RF, Lu DH, Jiang YH, Zhou R. Effect of cooling slope and manganese on the microstructure of hypereutectic Al-Si alloy with 2% Fe. *Mater Res.* 2014;17:511-7.
 8. Yu WB, Yuan ZH, Guo ZP, Xiong SM. Characterization of A390 aluminum alloy produced at different slow shot speeds using vacuum assisted high pressure die casting. *Trans Nonferrous Met Soc China.* 2017;27:2529-38.
 9. Vijian P, Arunachalam VP. Experimental study of squeeze casting of gunmetal. *J Mater Process Technol.* 2005;170:32-6.
 10. Lu CX, Zhou PF, Li TJ. Research on die casting performance of hypereutectic Al-Si alloy used in transmission fork. *Foundry.* 2017;66:1279-86.
 11. Fukui Y, Nara D, Kumazawa N. Evaluation of the deformation behavior of a semi-solid hypereutectic Al-Si alloy compressed in a drop-forge viscometer. *Metall Mater Trans, A Phys Metall Mater Sci.* 2015;46A:1909.
 12. Lin C, Wu SS, Lv SL, Wu HB, Chen HX. Influence of high pressure and manganese addition on Fe-rich phases and mechanical properties of hypereutectic Al-Si alloy with rheo-squeeze casting. *Trans Nonferrous Met Soc China.* 2019;29:253-62.
 13. Morita S, Yasuda H, Nagira T, Gourlay CM, Yoshiya M, Sugiyama A. Macroscopic modelling of semisolid deformation for considering segregation bands induced by shear deformation. *Mater Sci Eng.* 2012;33:1-8.
 14. Jin FW, Ren ZM, Ren WL, Deng K, Zhong YB, Yu JB. Effects of a high-gradient magnetic field on the migratory behavior of primary crystal silicon in hypereutectic Al-Si alloy. *Sci Technol Adv Mater.* 2008;9(2):1-8.
 15. Jiao XY, Wang J, Liu CF, Guo ZP, Tong GD, Ma SL, et al. Characterization of high-pressure die-cast hypereutectic Al-Si alloys based on microstructural distribution and fracture morphology. *J Mater Sci Technol.* 2019;35:1099-107.
 16. Chucheeep T, Wannasin J, Canyook R, Rattanochaikul T, Janudom SS, Wisutmethangoon S, et al. Characterization of flow behavior of semi-solid with low solid fractions. *Metall Mater Trans, A Phys Metall Mater Sci.* 2013;4754-63.
 17. Vieira EA, Ferrante M. Prediction of rheological behaviour and segregation susceptibility of semi-solid aluminium-silicon alloys by a simple back extrusion test. *Acta Mater.* 2005;53(20):5379-86.
 18. Beigi MTS, Niroumand B. Liquid segregation behaviour of a semi-solid squeeze cast A356 aluminium cup-shaped part. *Mater Sci Technol.* 2017;33:2203-11.
 19. Wang QP, Li L, Zhou RF, Li YK, Xiao F, Jiang YH. Rheological behavior of semisolid hypereutectic Al-Si alloys. *J Mater Res.* 2019;34:2105-13.
 20. Seo PK, Kang CG. The effect of raw material fabrication process on microstructural characteristics in reheating process for semi-solid forming. *J Mater Process Tech.*, 2005; 162-163:402-9.
 21. Zhang GZ, Yu XF, Wang XY, Jia GL, Gao YY. Non-equilibrium microstructure of Al-Si alloy solidified at superhigh pressure. *Chin Shu Hsueh Pao.* 1999;35(3):285-8.
 22. Evett JB, Liu C. *Fundamentals of fluid mechanics.* New York: McGraw-Hill; 1987. p. 381-390.
 23. Vinarcik EJ. *High integrity die casting process.* USA: John Wiley & Sons; 2003. p. 157-161.
 24. Mitsoulis E. *Flows of viscoplastic materials: models and computations.* *Rheology Reviews.* 2007;2007:135-78.
 25. Morris JF. A review of microstructure in concentrated suspensions and its implications for rheology and bulk flow. *Rheol Acta.* 2009;48:909-23.
 26. Lashgari I, Picano F, Breugern W, Brandt L. Laminar, turbulent, and inertial shear-thickening: regimes in channel flow of neutrally buoyant particle suspensions. *Phys Rev Lett.* 2014;113:254502-254502.
 27. Matas JP, Morris JF, Guazzelli E. Transition to turbulence in particulate pipe flow. *Phys Rev Lett.* 2003;90:014501.
 28. Hu XG, Zhu Q, Midson SP, Atkinson HV, Dong HB, Zhang F, et al. Blistering in semi-solid die casting of aluminium alloys and its avoidance. *Acta Mater.* 2017;124:446-55.